

See discussions, stats, and author profiles for this publication at: <https://www.researchgate.net/publication/360725118>

3D simulations of impulse waves originating from concurrent landslides near an active fault using FLOW-3D software: a case study of Çetin Dam Reservoir (Southeast Turkey)

Article in Bulletin of Engineering Geology and the Environment · May 2022

DOI: 10.1007/s10064-022-02738-4

CITATIONS

6

READS

400

4 authors:



Hakan Ersoy

Karadeniz Technical University

46 PUBLICATIONS 478 CITATIONS

SEE PROFILE



Muhammet Oguz Sunnetci

Karadeniz Technical University

24 PUBLICATIONS 202 CITATIONS

SEE PROFILE



Murat Karahan

Karadeniz Technical University

22 PUBLICATIONS 209 CITATIONS

SEE PROFILE



Dogan Perincek

Çanakkale Onsekiz Mart University

77 PUBLICATIONS 1,726 CITATIONS

SEE PROFILE



3D simulations of impulse waves originating from concurrent landslides near an active fault using FLOW-3D software: a case study of Çetin Dam Reservoir (Southeast Turkey)

Hakan Ersoy¹ · Muhammet Oğuz Sünnetci¹ · Murat Karahan¹ · Doğan Perinçek²

Received: 30 October 2021 / Accepted: 12 May 2022
© Springer-Verlag GmbH Germany, part of Springer Nature 2022

Abstract

This study used 3D numerical simulations to model the potential risk of impulse waves originating from concurrent landslides in Çetin Dam Reservoir in Southeast Turkey, which is near an active orogenic belt and related uplift system. A volume of fluid (VOF) model based on the Reynolds averaged Navier–Stokes equations was used to accurately simulate the free-surface/solid interaction, landslide deformation, and wave propagation. A renormalization group (RNG)-based $k-\epsilon$ turbulence model was used to create a fluid coupled model, and a drift-flux model was selected to simulate the potential landslide. A partially submerged landslide located 4900 m from the dam and another subaerial landslide located 800 m from dam were first modelled separately. 3D numerical models show that the impulse wave triggered by the subaerial landslide reaches 4 m in height at 34 s right in front of the dam, whereas the wave induced by the partially submerged landslide reaches 4.2 m in height at 205 s. After the effects of both landslides were modelled separately, the cumulative effect of impulse waves was evaluated in the case of the two landslides occurring simultaneously. As predicted, the highest wave reaching the dam body occurred 15 s later due to the interference of the two waves. However, contrary to expectations, the height of the new wave increased, which was probably due to the constructive interference of the original waves, and it reached 5.6 m at the dam body. Numerical analysis shows that when more than one landslide occurs simultaneously in the reservoir, the resulting interference affects the wave properties considerably.

Keywords FLOW-3D · Simulation · Impulse wave · Concurrent landslides · Dam reservoir

Introduction

Impulse waves are impact waves caused by glacial movements, avalanches, rockfalls, or landslides in dam reservoirs or natural water bodies, such as lakes, seas, and oceans. These natural phenomena are mostly triggered by earthquakes, volcanic activities, regional uplift-related morphologic changes, and climatic factors. The largest volcanic disaster events related to impulse waves ever recorded are those that formed as a result of the 1792 Unzen-Mayuyama landslide in Japan and the 1888 Ritter Volcanic Island collapse

in Papua New Guinea (Day et al. 2015; Wang et al. 2019). Similar cases have occurred in recent years. In 2002, the collapse of the northwest flank of a volcanic island in Italy created a 10-m-high wave, causing great damage to settlements on the coast of Stromboli Island (Bonaccorso et al. 2003; Di Risio et al. 2009).

The most striking example of landslide-induced impulse waves occurred in Alaska on July 9, 1958, which resulted in the largest recorded wave on earth. An earthquake developed by movement of the Alaska Fault caused a rock mass of approximately 40 million m³ to fall from a height of 950 m into the water on the north-eastern shore of Lituya Bay, which formed a 524-m-high impulse wave (Fritz et al. 2009). Historically, landslide-induced waves in areas of dam reservoirs have also had destructive effects. The most well-known example of this is a disaster that occurred in the reservoir area of Vajont Dam in 1963. A landslide occurred on the valley slope of the reservoir, resulting in a 250-m-high wave. This impulse wave breached the dam, resulting in the deaths

✉ Hakan Ersoy
ersoy@ktu.edu.tr

¹ Department of Geological Engineering, Karadeniz Technical University, Trabzon, Turkey

² Department of Geological Engineering, Çanakkale Onsekiz Mart University, Çanakkale, Turkey

of approximately 2,000 people in many towns downstream of the wave (Hendron and Patton 1987; Vacondio et al. 2013; Zhao et al. 2016).

The most recent cases of impulse wave-induced disasters in a reservoir area occurred in the Three Gorges Reservoir in China after 2008 (Zhang et al. 2010). These include the 2008 Gongjiafang landslide in Wu Gorge, the 2010 Qingshi landslide on the Yangtze River, and the 2015 Hongyanzi landslide in Wushan (Yin et al. 2015). These landslide-induced impulse waves caused many casualties and millions of dollars of economic losses.

Following many catastrophic events caused by landslides in reservoir areas, increased attention is focused on studies of the mechanisms of landslide formation, landslide stability in dam-construction areas, and effects of landslide tsunamis in reservoirs. Generally, studies on the effects of landslide-induced impulse waves in reservoirs consist of two basic types. The first involves the determination of the properties of the landslide material that creates the impulse wave—that is, boundary conditions such as the thickness, width, density, and slide impact velocity, as well as the bulk slide volume that enter the reservoir. The second type of study involves modelling the formation and propagation of impulse waves.

Many investigations about the propagation and formation mechanism of landslide-induced impulse waves have gained attention in the last decades. Studies have addressed the landslide-generated waves using three main approaches to determine their physical properties, to evaluate their generation and propagation in reservoirs, and to investigate the effect on reservoir shores and structures, such as the dam body (Zhang et al. 2020). The first approach is to use empirical equations developed from model tests (Hughes 1993; Heller and Hager 2010; Heller et al. 2009; Bregoli et al. 2017) or derived from field data (Fritz et al. 2004; Quecedo et al. 2004). Second, specific experiments are done using a physical hydraulic model or prototype that realistically reflects the topography (Wang et al. 2019; Liu et al. 2005). The third approach involves 2D or 3D numerical simulation models (Grilli et al. 2002; Montagna et al. 2011; Gabl et al. 2015; Li et al. 2019; Xu et al. 2020).

Due to the development in computer and software technologies, the numerical simulations have become almost essential to analysis of the generation and propagation of water waves such as tsunamis on coastal areas (Smith et al. 2016; Bazykina et al. 2018; Abdollahi and Mason 2019) and impulse waves in dam reservoirs (Yavari-Ramshe and Ataie-Ashtiani 2016; Evers and Hager 2015; Karahan et al. 2020a). Many investigations based on 2D or 3D numerical simulations have been conducted to predict the characterisation of landslide-generated impulse waves in the last decade due to their ability of determining the wave parameters at any desired location (Wang et al. 2019; Zhang et al. 2020; Li et al. 2019;

Heller et al. 2016; Ersoy et al. 2019; Huang and Wang 2017). Different numerical models have been carried out in these investigations to predict the generation of landslide-induced impulse waves which are the smoothed particle hydrodynamic (SPH) model (Wang et al. 2015; Shi et al. 2016), computational fluid dynamics (CFD) and volume of fluid (VOF) methods (Montagna et al. 2011; Li et al. 2019), and discrete element methods (DEM) (Zhao et al. 2016; Xu et al. 2020; Kessler et al. 2018). Detailed determination of the boundary conditions of a landslide is crucial for the consistency of wave propagation models. However, almost all numerical studies on landslide-induced impulse waves have mostly focused on existing landslide cases due to the availability of various data recorded in a natural environment about landslide cases and wave propagation. These existing data are used directly in analytical and numerical analyses to verify models (Wang et al. 2019; Zhao et al. 2016; Yin et al. 2015). Thus, studies to predict the propagation of waves that could be formed by a probable landslide on reservoir slopes are extremely limited to a few important studies (Montagna et al. 2011; Li et al. 2019; Ersoy et al. 2019, 2020; Xu et al. 2020, 2021; Karahan et al. 2020b; Wang et al. 2020).

Unlike the studies mentioned above, many investigations on impulse or tsunami waves were carried out to investigate wave interference effects and the effect of reservoir geometry on wave propagation. Shen et al. (2022) presented an analytical model based on linear wave theory and a Reynolds-averaged Navier–Stokes (RANS) model based on OpenFOAM to study the effect of segmented seabed deformations on the wave generation process. A single segment, two opposing segments, and three opposing segments were used as representative scenarios, and the authors concluded that waves generated by a single uplifting or subsiding segment are always the largest. The maximum wave height decreases by 40% from the scenario with a single segment to the scenario with two equal-sized segments, and there were further decreases by 39% from the scenario with two segments to the scenario with three segments.

Kafle and Tuladhar (2018) indicated that higher impulse wave heights are caused by reflection, interaction, and interference. The study indicated that the reflection and intersection of coupled three-dimensional tsunami waves observed as a partially submerged two-phase debris mass impact the quiescent water reservoir. Franco et al. (2021a, b) studied the 3D dynamic reconstruction of the Taan Fiord 2015 tsunami event in Alaska. The landslide's evolution and the impulse wave dynamics of the event were studied in detail using the numerical software Flow3D. One of the important results was that reflected waves play a main role in the water reaching high parts on steep slopes. Zhang et al. (2020) performed 14 numerical experiments using the Tsunami Squares method to investigate the effect of reservoir geometry on the propagation properties of landslide-generated impulse waves

in two different reservoir shapes: converging and diverging. The results indicated that wave amplitudes decrease with increasing reservoir width and that wave decay is more affected by the diverging reservoir geometry.

As in the studies mentioned, when modelling the formation, propagation, and interference of impulse waves, the effect of a single source is usually considered. Unlike studies on earthquake-induced tsunamis, a single mass is generally modelled in many studies on impulse waves. However, even a single mass can create more than one wave in a water body, regardless of the cumulative effect. Figure 1 shows the three phases of impulse wave development above a horizontal reservoir bed (Heller et al. 2009): (1) wave generation, (2) wave propagation in the water body, and (3) impact, run-up, and, in some cases, overtopping. As shown in Fig. 1, more than one impulse wave is formed as a result of a landslide. However, almost all studies consider the propagation of the highest wave, which occurs with the first impact.

Similar to the formation of many waves as a result of a single landslide, in the case of many landslides during an earthquake, multiple waves propagating in different directions may also occur. The waves can dampen each other (destructive interference), or a new wave with increased height can form (constructive interference). In this case, a model made for a single landslide and single wave will not be valid. Therefore, in this study, the aim was to evaluate the cumulative effects of impulse waves originating from concurrent landslides.

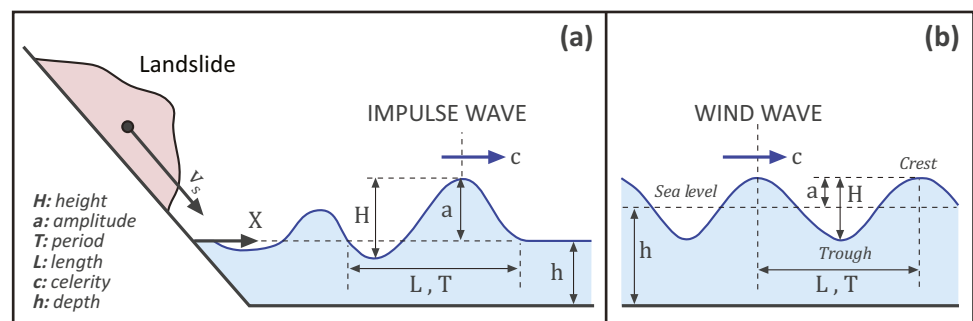
There are not many investigations on the estimation of the effects of impulse waves triggered by landslides that have not yet occurred but pose a risk. Furthermore, studies evaluating the cumulative effects of impulse waves that could be induced by more than one landslide are extremely limited. However, more than one landslide may occur at the same time in reservoirs where there is a risk of landslides on their slopes especially because of heavy precipitation or earthquakes. The Çetin Dam Reservoir area located in the south-eastern part of Turkey is a striking example of this situation.

The Çetin Dam was built on the Botan Stream, the largest tributary of the Tigris River, and started operating in 2020. The dam is located 15 km west of Pervari district (Siirt) and is a roller-compacted-concrete dam. The crest altitude of the dam is 825 m, and the maximum water level is 822 m (the operation water level is 820 m). After impoundment, toes of many landslides in the basin partially have submerged into the reservoir of the dam. Not only are there many active landslides in the dam reservoir area, the dam body and reservoir are located 10 km north-east of an active thrust-fault zone (Fig. 2).

It is very well known that seismic activities are especially dominant near active fault zones, and they affect vast areas on the surface. In this regard, simultaneous reactivation of multiple paleo-landslides in dam-lake areas is a valid concern. Extensive studies have been done on the seismic response of soil slopes and concrete-faced rockfill dam slopes (CFRD). These studies have used a finite element time-history method and a novel stochastic method (generalized probability density evolution method, GPDEM) to assess plastic deformations induced by seismicity (Li et al. 2021a, b; Pang et al. 2018, 2021). However, this study does not focus on the triggering mechanisms of the landslides or deformations occurring within the dam body due to seismicity.

The Çetin Dam reservoir was chosen for this study because there are many active landslides on the reservoir slopes, and it is very close to an active fault zone, so there is a risk of concurrent landslides occurring during an earthquake. In this case, it is necessary to investigate the cumulative effects of landslide-induced impulse waves rather than the effect of a single wave. Thus, the present study focuses on the cumulative effects of impulse waves on the dam body and reservoir shores in the case of two landslides with 3D numerical simulations. For this purpose, the volume of fluid (VOF) method based on computational fluid dynamics (CFD) was used to accurately predict the impacts of high-velocity slides and complicated solid–free surface (water) boundary transformations.

Fig. 1 The three phases of an impulse wave above a horizontal reservoir bed (Heller 2007)



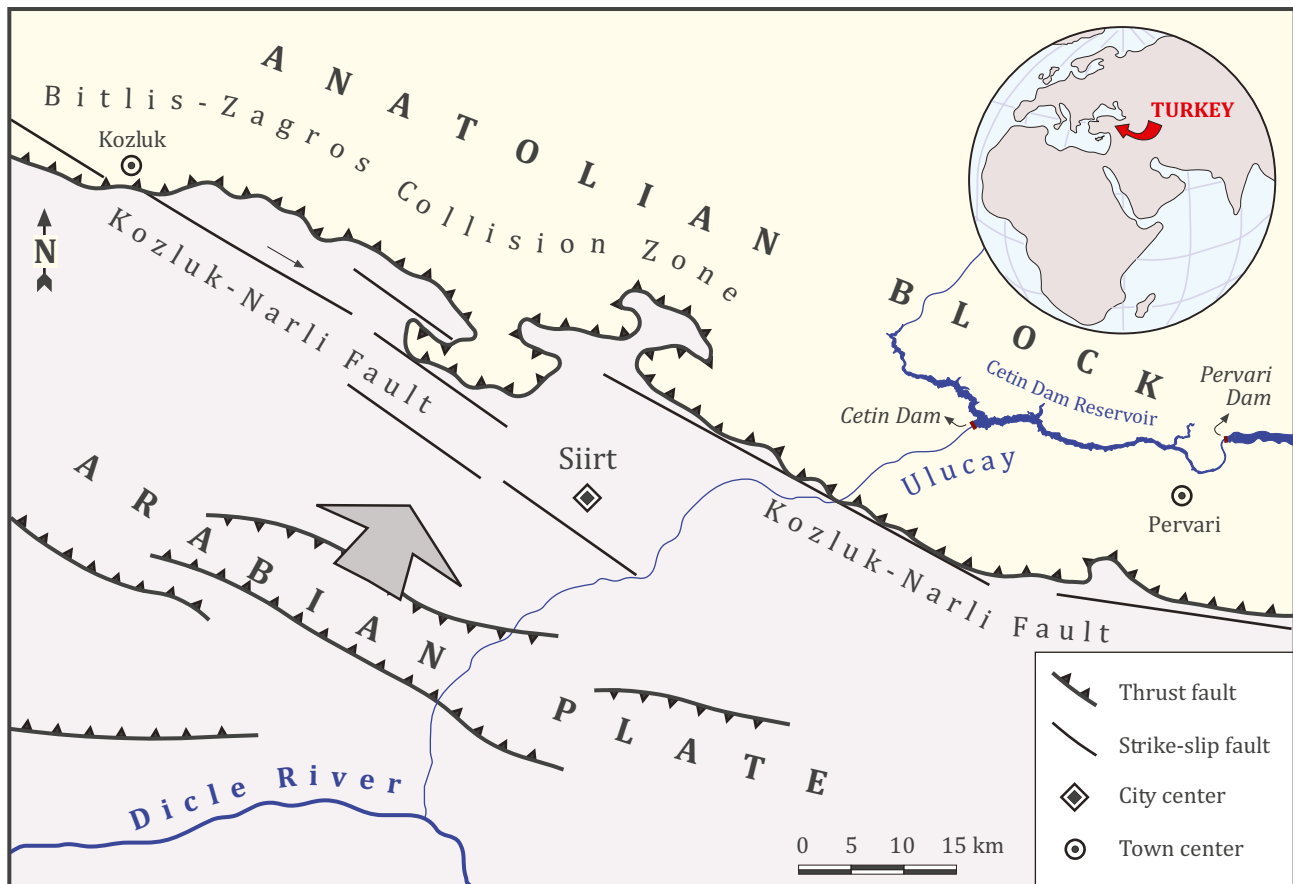


Fig. 2 Tectonic structures around the studied area (modified from Utmanoğulları 2012)

FLOW-3D software based on the 3-D RANS equations and the renormalization group turbulence model were used.

Geological setting and tectonic properties

The study area is located in a transition zone between the Arabian and Taurus plates (Açıkbaş et al. 1981). Tectonic activities influenced the region from Palaeozoic to Late Miocene. The Bitlis-Zagros Thrust Belt and Kozluk-Narlı Fault are the most dominant of many Plio-Quaternary faults controlling the tectonic properties of the study area and its vicinity (Fig. 2). The slip of this right lateral strike-slip fault varies between 800 and 1200 m (Perinçek et al. 1987). The morphological elements formed by the Narlı-Kozluk Fault (Perinçek et al. 1987), which extends parallel to the Miocene thrust zone (Bitlis-Zagros Suture Zone) in the southern part of the study area, can be seen very clearly. The Botan Stream flows for 3–4 km through a valley which is formed under the control of the weakness zone caused by the Narlı-Kozluk Fault. The angles of

the slopes are very high along the Botan Stream (Uluçay) valley, where the study area is located. Tectonic activities causing Southeast Anatolian thrust belt to be compressed in the north–south direction since Middle Miocene is the main reason of these steep slopes. Compression is met by reverse faults and strike-slip faults and the region is constantly rising. The most important of the many data showing the continuous uplift of the region are the suspended old riverbed erosion plains and terraces.

In the study area, most of the units outcropping in the region where intense tectonic activities developed are allochthonous and were transported to the region at different geological times (Fig. 3). The Early-Middle Eocene aged Maden Complex (Perinçek 1990; Yılmaz and Yiğitbaş 1990) is characterized by basalt, andesite, spilite and diabase dykes. In the upper parts of the formation, there are limestone, clayey limestone, and clay stones. The upper and lower boundaries of the Maden Complex are generally tectonic. The Palaeozoic-Mesozoic aged Bitlis Metamorphic (Tolun 1954) which overlay Maden Complex by thrust faults generally consist of mica schists, phyllites

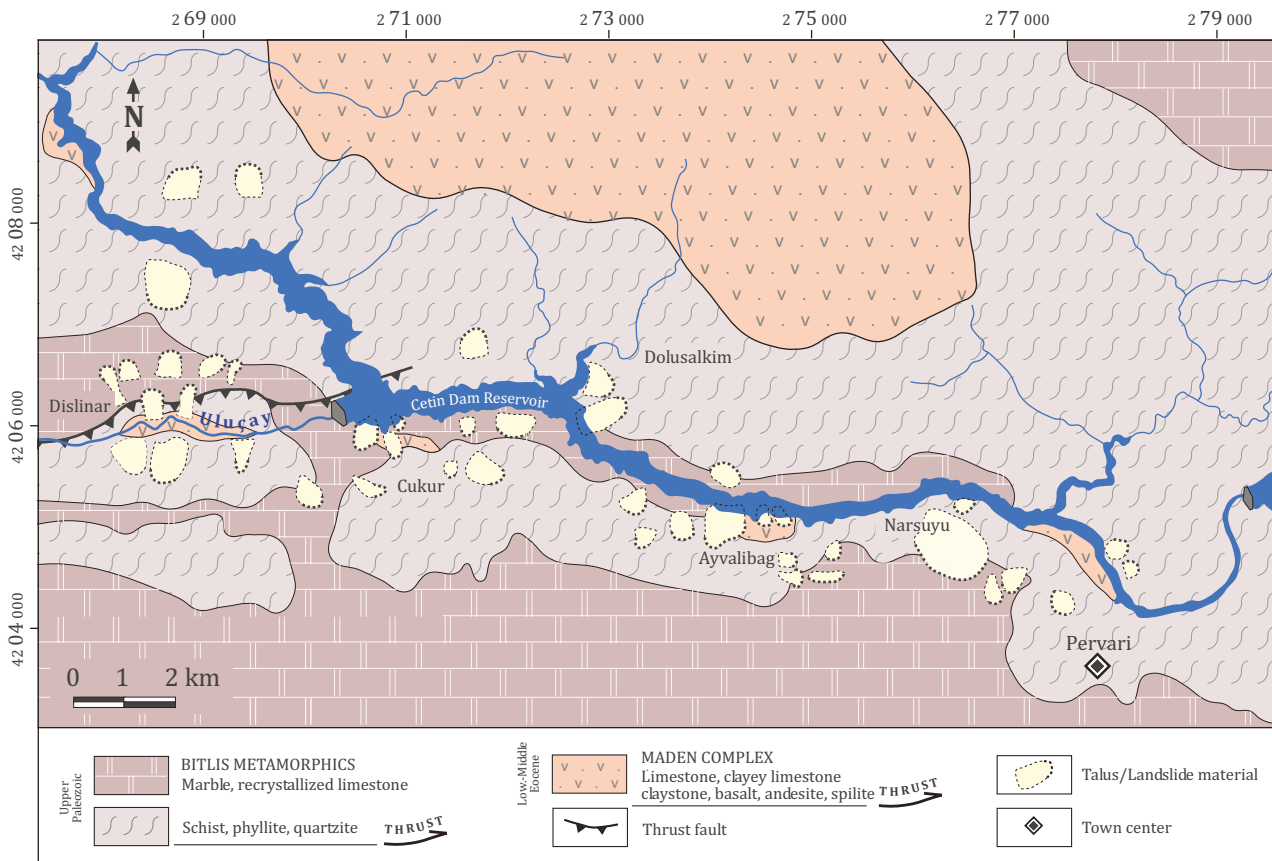


Fig. 3 Geological map of the studied area (modified from Perinçek 2016)

and quartzites. In the upper parts, crystallized limestones and marbles are dominant (Perinçek 1980).

Landslide potential

Çetin Dam was built in the Botan Stream (Uluçay) Valley, where the slopes are very steep. There are many active and paleo-landslides in the reservoir area. Steep slopes are one of the most important reasons for landslides. In addition, landslides occur when overlying metamorphic rocks slide towards the valley along shear surfaces formed by the saturation of claystone and clayey limestone layers, especially in localities where Bitlis metamorphic rock overlays the Maden Complex with thrust faults. Active tectonism, lithology, morphology, and climatic properties of the region increase the risk of landslides. Hence, in the case of a landslide due to an earthquake or sudden heavy precipitation in the dam reservoir, landslide-generated impulse waves can threaten the dam body and settlements near the reservoir area (Perinçek 2016). In addition, it is of great importance to determine the risks due to the cumulative effects of impulse waves that will occur

because of the movement of multiple landslides together into the reservoir.

After the dam construction was planned, studies on landslides in the region increased. In a detailed study by Perinçek (2016), many landslides were mapped along the reservoir area near the villages of Çukur, Ayvalibağ, and Narsuyu. The cause of the landslides in the northeast of Çukur Village is the Maden Complex outcropping in the northwest of the village. The Maden Complex is covered by landslide material in the east. The toe sections of some active landslides in this vicinity are partially submerged in the dam reservoir. Because metamorphic rocks that outcrop just below the landslides form a natural barricade, there is no risk of these landslides creating impulse waves. In this region, only the landslides located within the mudstones and clayey units belonging to the Maden Complex at higher elevations than the reservoir level carry great risk (Fig. 3).

There are several active landslides along the reservoir to the northeast of Pervari and around the village of Narsuyu. In addition, active landslides in the region are located around the villages of Ayvalibağ. The most important reason for the formation of these landslides is the steep slopes. The second

reason is the mudstone layers in the Maden Complex (Perinçek 2016). Because of factors such as the reservoir geometry and the distance to the dam body of landslides (more than 10 km), impulse waves generated from these landslides are thought to have very small effects in this region.

The landslide risk is lower on the right bank of the reservoir, especially on the northern slopes. However, the toe of an active landslide located in the southwest of Dolusalkım Village is submerged in the reservoir (Fig. 4). If this landslide enters the reservoir, the generated impulse wave will directly affect the dam body negatively (Perinçek 2016).

Establishment of geological model

This study investigated the cumulative effects of impulse waves that could occur in cases of more than one landslide. The simultaneous effects of waves from the subaerial active landslide near Çukur Village and a partially submerged landslide near Dolusalkım Village were evaluated (Fig. 3). In previous studies, the characteristics of both landslides were determined in detail as a result of evaluating data obtained from aerial photographs and field studies whole (Perinçek 2016).

Landslide 1 developed within the talus that outcrops between elevations of 1100 and 800 m and had a width of approximately 300–350 m. The toe of the landslide is located on the left bank approximately 800 m from the dam body at an elevation approximately 50 m above the reservoir (Fig. 4). The landslide has an average width of 140–150 m and extends up to an elevation of 992 m. As a result of field observations, it is estimated that the thickness of the landslide varies from 10 to 12 m.

Landslide 2 developed within the talus that outcrops in a very wide area on the right bank 4900 m away from the dam body (Fig. 4). Slope debris outcrops up to an elevation of

1250 m, but the landslide is located at elevations lower than 1000 m. The toe of the landslide material has an average width of 290–300 m and a thickness of approximately 15–17 m and is submerged under the reservoir water.

Creation of 3D solid body model

In the scope of the study, raster-based 1/25,000 scaled digital topographic maps were used to create a 3D solid model of reservoir area, and this data was converted to a point cloud database using ArcGIS (10.3) and NetCAD GIS software (7.6). A total of 4,434,129 points in the database were converted to a text file format, and 3D solid model in stereolithography (STL) files were transferred to the FLOW-3D software. Also, the created dam body and landslide material were placed on the 3D solid model.

Solid dam body model was created using SolidWorks which is a CAD software for creating 2D and 3D solid models in a simple, fast, and efficient way. The 3D Sketch feature providing convenience in drawing 3D models was used in the software. The 3D dam model is shown in Fig. 5.

For numerical solutions of the propagation of impulse waves on a rigid solid body, mesh blocks containing rectangular cells were selected for easy generation and computation. Initial time steps and grid resolution directly affect the numerical results. For this reason, FLOW-3D was used because it can solve this challenge by dividing the domain into several grids of different resolutions and uses nested grids (De-Girolamo et al. 2009; Kim 2012). The reservoir area is approximately 21 km² and was defined with 68,857,800 uniform cells of 6 m × 6 m. Neumann boundary conditions were also selected. In the model, water with a density of 1,000 kg/m³ was used as fluid, and the topography surfaces were modelled as

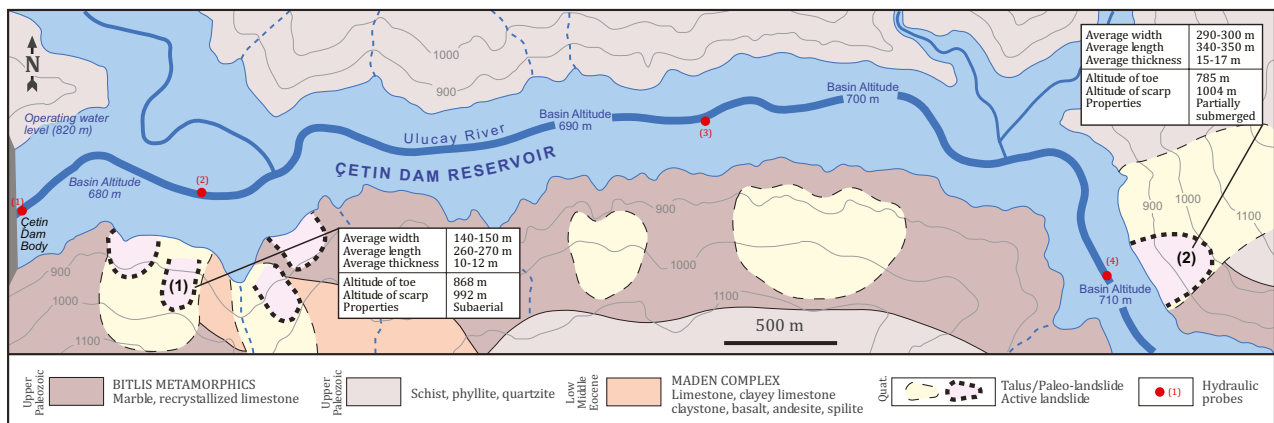
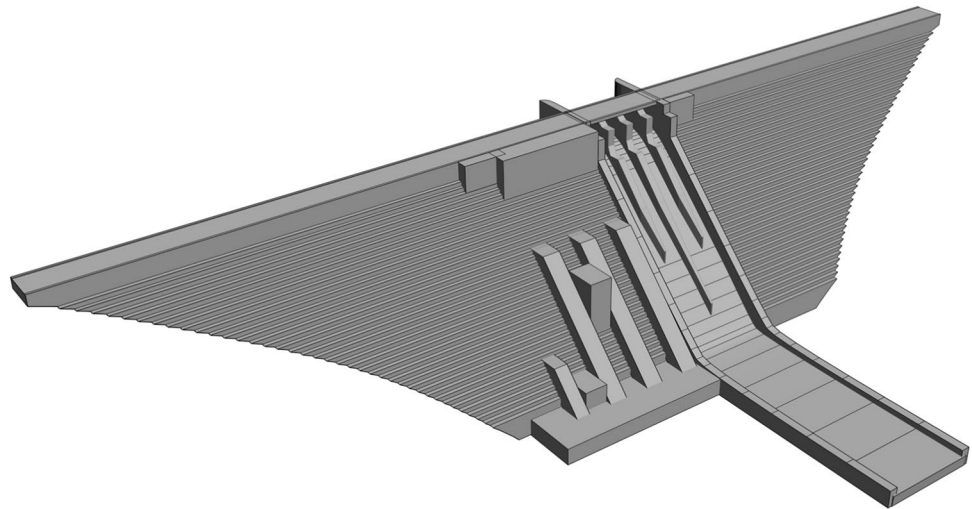


Fig. 4 Detailed geological map including active landslide around the Çetin Dam Reservoir (modified from Perinçek 2016)

Fig. 5 3D solid model of the Çetin Dam



non-friction and impermeable walls. The total time of the 3D simulation was selected as 250 s. Table 1 shows the physical properties and boundary conditions of the parameters used in the numerical model.

Hydrological model

Numerical methods such as the finite element, finite difference, and finite volume methods are used to approximate the governing equations in mathematical models and

are generally used in many engineering areas. In hydraulic model-based studies, fluid motion is governed by the Navier–Stokes equations, which are a set of coupled and nonlinear partial differential equations derived from the basic laws of conservation of mass, momentum, and energy. Obtaining an analytical solution of these equations is practically impossible. Thus, CFD methods use numerical analysis and data structures to analyse and solve problems that involve fluid flows in hydraulic model-based studies.

FLOW-3D is general-purpose CFD software that employs specially developed numerical techniques to solve the

Table 1 The boundary conditions of the 3D numerical models

Topographical surface	<p>Solid model: 1/10,000 digital elevation model (4,434,129 points to text file from cloud point)</p> <p>Surface geometry: stereolithography (STL) files</p> <p>Surface model: impermeable wall</p>
Model geometry and boundaries	<p>Total number of real cells: 68,857,800</p> <p>Size of cells: 6 m × 6 m</p> <p>Mesh type: non-conforming</p> <p>Model boundary: Xmin, Xmax, Ymin, Ymax, Zmin: Solid wall Ymax and Zmax: Outflow</p> <p>Free surface elevation: Z high 820 m</p>
Hydraulic model	<p>Activate gravity z component: -9.81 m/sn^2</p> <p>Viscous flow: Renormalized group (RNG)</p> <p>Model: two-equation ($k-\epsilon$) model</p> <p>Activate: Drift-flux model</p>
Reservoir water	<p>Fluid temperature: 20 C°</p> <p>Dynamic viscosity: $1.002 \text{ (Ns/m}^2) \times 10^{-3}$</p> <p>Specific volume: $0.001002 \text{ m}^3/\text{kg}$</p> <p>Specific heat: $4.183 \text{ kJ/kg } ^\circ\text{C}$</p> <p>Density: 1000 kg/m^3</p>
Landslide material and dam body	<p>Landslide: Water at 20 °C and density: 1500 kg/m^3</p> <p>Dam body: 1/500 scaled 3D solid model in STL file</p>
General properties	<p>Simulation time: 250 s</p> <p>Number of fluids: one fluid with different density</p> <p>Simulation unit: SI</p> <p>Temperature units: Celsius</p> <p>Probes: 4 probes on water above water</p>

equations of motion for fluids to obtain transient, three-dimensional solutions to multi-scale, multi-physics flow problems. This software is based on solving the RANS equations using finite difference and finite volume methods. The two most popular methods in geohazard reconstruction are the shallow equation method (SEM) and the discrete element method (DEM). SEM uses the conservation equations of mass, momentum, and energy to quickly reconstruct the behaviour of landslides or debris flows. In this study, continuum-based SEM was used.

The wave generation was simulated using a free-surface modelling technique with a VOF model based on the RANS equations. A renormalization group (RNG)-based $k-\varepsilon$ turbulence model was used to create a fluid–fluid coupled model. In addition, a drift-flux model was selected to simulate potential landslides.

Drift-flux model

For fluids consisting of multiple components, such as liquid and particles, the flow velocities may differ for each of these components. Non-uniform body forces based on the difference in densities are generally the main reason for these flow-velocity differences. However, the relative speeds are low enough to be described as a “drift” among components under different conditions. The “drift” distinction is related to whether the inertia of a dispersed component moving continuously in a component is substantial. A “drift-flux” approach is applied when the inertia of relative motion can be ignored, and the relative speed is reduced due to an equilibrium between a pressure gradient and an opposing drag force between the components. Drift velocities are primarily responsible for the transport of mass and energy (Brethour and Hirt 2009).

The drift-flux model can be appropriately used when the motions of two phases are strongly coupled. The drift-flux model is very important because of its simple application to a broad range of two-phase flow problems of practical interest (Hibiki and Ishii 2003). The drift-flux model has several advantages over a multi-fluid model. The drift-flux model includes momentum equations, so it requires less CPU time for calculations, in contrast to multi-fluid models, which must deal with two (gas and liquid) or three (gas, oil, and water) different momentum equations (Spesivtsev et al. 2013). The formulation of the relative velocity in the drift approximation proceeds as follows: define $u = f_1 u_1 + f_2 u_2$ such that $\bar{V}u = 0$ for the incompressible flow of a two-component fluid. The volume of fractions of the two components making up a mixture is specified by f_1 and f_2 where $f_1 + f_2 = 1$:

$$\frac{\partial u_1}{\partial t} + u_1 \bar{V}u_1 = -\frac{1}{\rho_1} \bar{V}P + F + \frac{K}{f\rho_1} u_r \tilde{V} \quad (1)$$

while for the dispersed phase, it is

$$\frac{\partial u_2}{\partial t} + u_2 \bar{V}u_2 = -\frac{1}{\rho_2} \bar{V}P + F - \frac{K}{(1-f)\rho_2} u_r \quad (2)$$

where:

u_1 and u_2 : the microscopic velocities of the continuous and dispersed phases

f : the volume fraction of the continuous phase

F : body force

K : drag coefficient related to the interaction of the two phases

$u_r (u_2 - u_1)$: difference relative velocity between dispersed and continuous phases

The drift flux model aims to compute the motion of the two phases relative to the volume-averaged velocity (\bar{u}). The volume-weighted average velocity is $\bar{u} = f u_1 + (1 - f) u_2$. The volume-weighted average velocity is chosen from the mass-weighted average due to automatically enforced mass continuity. Some momentum may be transported as well, but this is usually quite small and has been neglected in the FLOW-3D drift model.

A talus generally presents a granular structure, and therefore, the failure surface is generally circular in landslides that occur in a talus. Field observations made in this study, topographic features of the study area, and its geological structure show that the failure surface of the landslide that may develop in the talus may be planar. For this reason, there may be a flowing movement rather than sliding in the talus, and this situation could be modelled realistically with the drift-flux model. As in many studies, the reservoir water is defined as a fluid with a density of 1000 kg/m³, and the landslide material is defined as a fluid with a density of 1500 kg/m³. Thus, the drift–flux model for two-phase-flow analysis was used in the study.

RANS solution with RNG $k-\varepsilon$ turbulence model

Landslide-induced impulse waves often make water flow turbulent in a dam reservoir. A superimposed high-frequency random fluctuation is a characteristic feature of this type of flow. Numerous turbulence models can be used to determine turbulence viscosity in computational fluid dynamics (Kocaman and Ozmen-Cagatay 2015), but the RNG $k-\varepsilon$ turbulence model based on instantaneous Navier–Stokes equations was used here because it is a more robust version of the two-equation $k-\varepsilon$ model. In addition, the model increases the capabilities of the standard $k-\varepsilon$ model to carry out better coverage of transitionally turbulent flows and mass transfer.

This model was created using a mathematical formulation called “renormalization group” (RNG) methods. Although the RNG $k-\epsilon$ model has a similar form to the standard $k-\epsilon$ model, unlike the standard $k-\epsilon$ model, the RNG theory provides an analytically derived differential formula for effective viscosity that accounts for low-Reynolds number effects.

$$\frac{\partial}{\partial t}(\rho k) + \frac{\partial}{\partial x_i}(\rho k u_i) = \frac{\partial}{\partial x_j} \left(\alpha_k \mu_{eff} \frac{\partial k}{\partial x_j} \right) + G_k + G_b - \rho \epsilon - Y_M + S_k \tag{3}$$

$$\frac{\partial}{\partial t}(\rho \epsilon) + \frac{\partial}{\partial x_i}(\rho \epsilon u_i) = \frac{\partial}{\partial x_j} \left(\alpha_\epsilon \mu_{eff} \frac{\partial \epsilon}{\partial x_j} \right) + C_{1\epsilon} \frac{\epsilon}{k} (G_k + G_{3\epsilon} G_b) - C_{2\epsilon} \rho \frac{\epsilon^2}{k} - R_\epsilon + S_\epsilon \tag{4}$$

where

G_k : generation of turbulence kinetic energy because of the average velocity

G_b : generation of turbulence kinetic energy because of buoyancy

Y_M : fluctuating dilatation contribution in compressible turbulence

$\alpha_k, \alpha_\epsilon$: Prandtl numbers for k and ϵ

S_k, S_ϵ : user defined source terms

C_ϵ : a coefficient value (Choudhury 1973)

Because FLOW-3D is a computational fluid dynamics (CFD) software, it uses the equations (Eqs. (1), (2), (3), and (4)) specified here in the solution of the numerical analysis.

3D simulations of landslide-generated impulse waves

Landslide-triggered waves in reservoir areas generally propagate according to the principles of turbulent flow and are characteristic of this type of flow, which represents “superimposed high-frequency random fluctuation.” FLOW-3D was used in

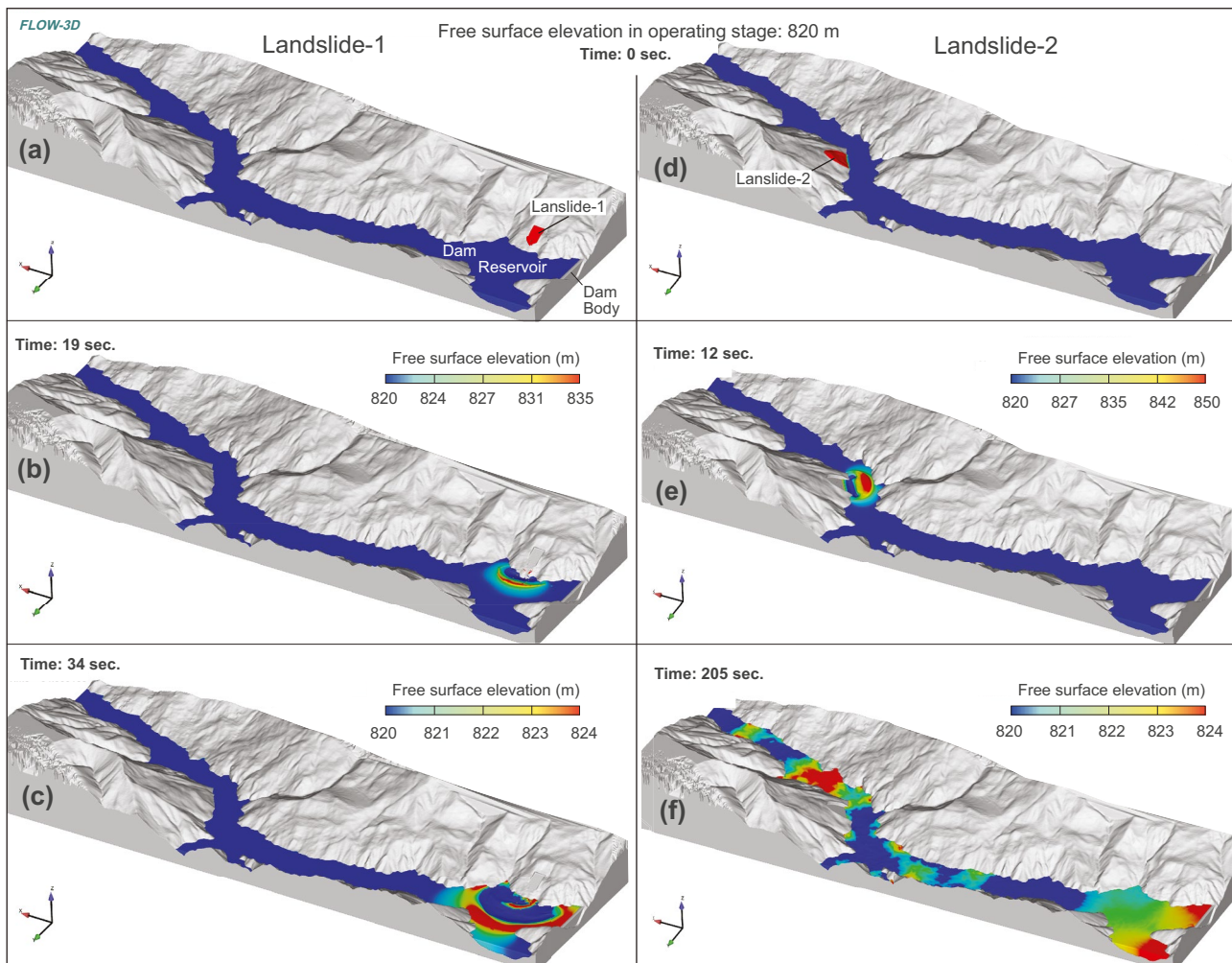
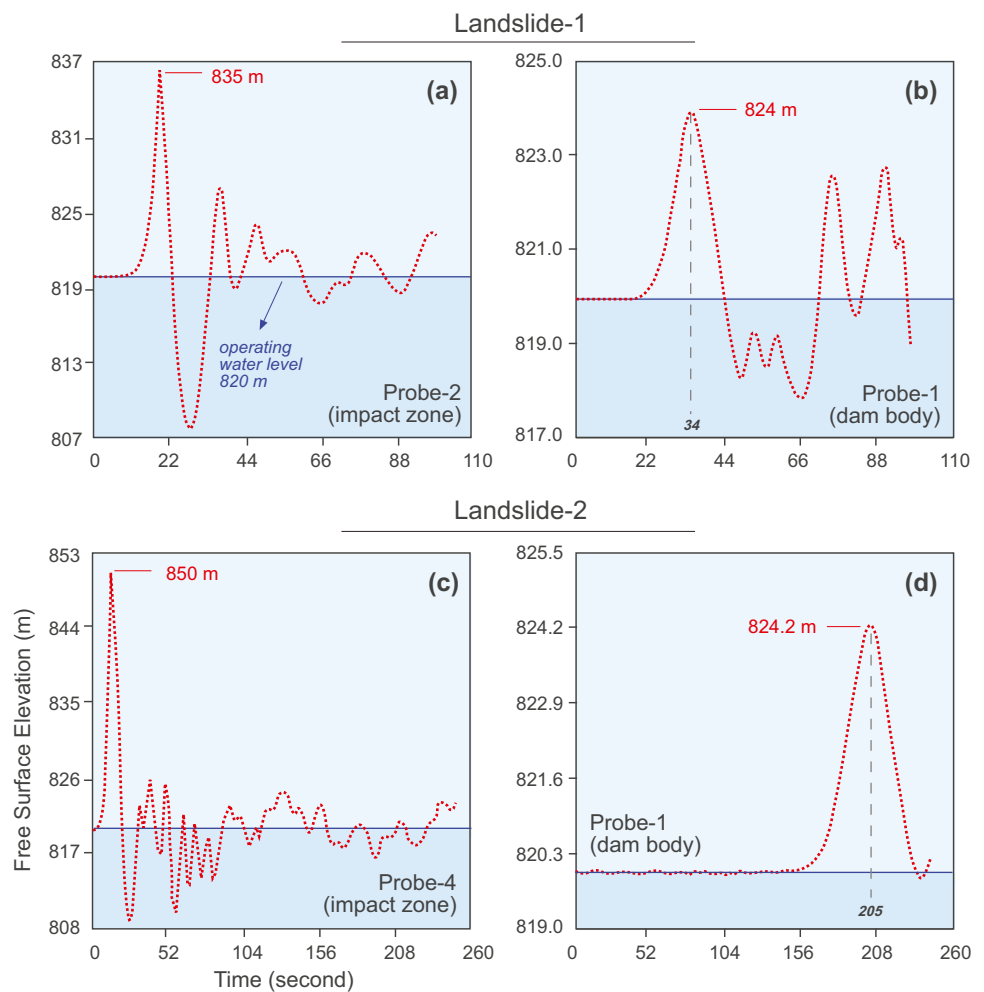


Fig. 6 Exemplary results of the simulation by FLOW-3D (including added original STL geometry) of two landslides separately and impulse wave formation model between 0 and 34 s for Landslide 1, between 0 and 222 s for Landslide 2

Fig. 7 Surface water elevation (a at impact zone at the 17th second for the Landslide 1, b near the dam body at the 34th second for the Landslide 1, c at impact zone at the 15th second for the Landslide 2, and d near the dam body at the 205th second for the Landslide 2)



this study because it efficiently simulates both propagation of regular linear and nonlinear surface waves, as well as irregular waves. This software is a CFD programme that was developed to solve fluid motion equations. The programme can simulate the 3D movement of landslide material in reservoir areas and the propagation of landslide-induced impulse waves (Montagna et al. 2011; Gabl et al. 2015; Ersoy et al. 2019).

Because FLOW-3D presents the time-height and time-velocity data along a line, the properties of the impulse waves are recorded anywhere in the reservoir during the propagation, both spatially and temporally. 3D numerical simulations were created over 250 s, and the impulse wave propagation was simulated for different timespans. In addition, some probes were placed on the reservoir during the wave propagation time at different distances from the landslide area. Two of them were placed in front of the slide impact zone for two landslides, another was placed between the two landslides, and the last one was placed just in front of the dam body.

In the first phase of the study, activation of Landslide 1 was simulated (Fig. 6a–c). The numerical analysis showed that the landslide reached the reservoir within 7 s after its formation, and all the landslide material (approximately 400,000 m³) slid into the reservoir within 19 s (Fig. 6b). A 15-m wave (Figs. 6b and 7a) formed in the impact area and was dampened by hitting a ridge just west of the impact area and extending to the reservoir. It reached the dam body in 34 s. The surface-water elevation at Probe 1 in front of the dam body was measured as 824 m, and the wave height was 4 m (Figs. 6c and 7b).

In the second phase of the study, activation of Landslide 2 was simulated (Fig. 6d–f). In this case, it took 12 s for approximately 1.5 million m³ of landslide material to completely slide into the reservoir (Fig. 6e), and some of the material remained in the reservoir water. The height of the wave that formed in the impact area was recorded as 30 m at Probe 4 (Fig. 7c). The resulting wave travelled 4900 m along the reservoir and reached the dam body after 205 s (Fig. 6f).

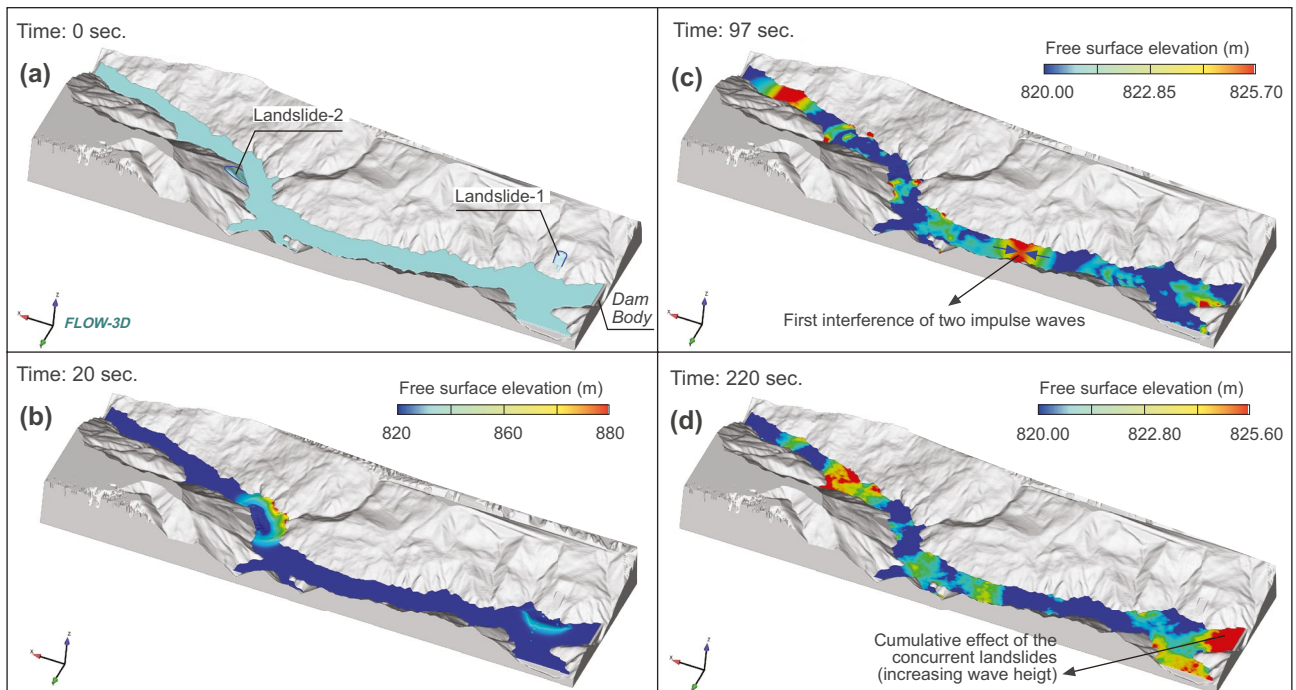


Fig. 8 Exemplary results of the simulation by FLOW-3D (including added original STL geometry) of the concurrent landslides and impulse wave formations model between 0 and 220 s

The surface-water elevation at Probe 1 was recorded as 824.2 m, and the wave height as 4.2 m (Figs. 6f and 7d).

In the last phase of the study, the effect of concurrent landslides was simulated (Fig. 8). Impulse waves were formed by the landslides and propagated towards each other (Fig. 8b), and the waves have interfered with each other at 97 s. The wave height was recorded as 5.7 m at Probe 3 at the location of the interference (Fig. 9a). However, the wave heights recorded at Probe 3 when the landslides occurred separately were 0.95 m and 4.7 m for Landslide 1 and Landslide 2, respectively (Fig. 9a). The resulting constructive interference at the point of collision is thought to be the

main reason for higher wave heights recorded at Probe 3 in the case of concurrent the landslides.

Another important result obtained is that if two landslides occurred simultaneously, the surface water elevation measured at the dam body reached 825.6 m, and the wave height reached 5.6 m after 220 s (Figs. 8d and 9b). When both landslides occurred separately, the measured surface water elevations at the dam body were 820.95 m and 824.2 m for Landslide 1 and Landslide 2, respectively. In this case, even though the waves were expected to dampen each other, the height of the impulse wave after interference increased to 5.6 m at the dam body (Fig. 9b).

Fig. 9 Surface water elevation (a for Landslide 1, Landslide 2, concurrent landslides in the Probe-3 at the 97th second, b for concurrent landslide near to dam body in the Probe-1)

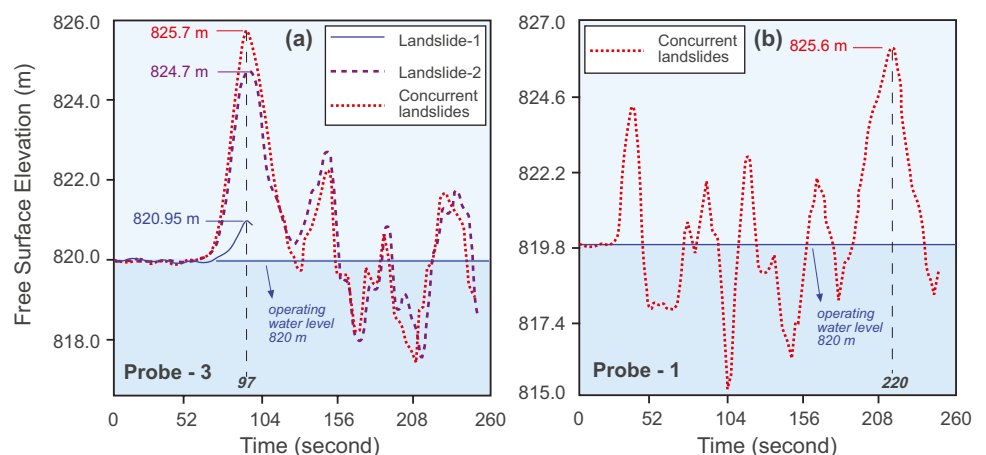


Table 2 Surface water elevation and wave height values recorded at different probes in case landslides occur at different times or at the same time

Probe No	Water column (m)	Landslides		
		Landslide 1	Landslide 2	Concurrent
Probe-3 (interference location)	Surface water elevation	820.95	824.60	825.70
	Wave height	0.95	4.70	5.70
Probe-1 (dam body)	Surface water elevation	824.00	824.20	825.60
	Wave height	4.00	4.20	5.60
Probe-2 (impact zone of Landslide 1)	Surface water elevation	835.00	-	-
	Wave height	15.00	-	-
Probe-4 (impact zone of Landslide 2)	Surface water elevation	-	850.00	-
	Wave height	-	30.00	-

Discussion and conclusion

Compared to the initial damage caused by natural disasters, more damage can sometimes be caused by mass movements triggered by natural events such as earthquakes, excessive precipitation, or volcanic activity. With the effect of such natural disasters, multiple mass movements can occur at the same time in areas that are very close to each other. The cumulative effects of impulse waves created by more than one landslide formed around water bodies such as dam reservoirs, lakes, fjords, and gulfs may pose great risks. For this reason, it is of great importance to investigate the holistic effects of impulse waves that could occur in cases of more than one landslide, especially in dam reservoir areas located near tectonically active zones.

The Çetin Dam Reservoir is located near a transition zone between the Arabian and Taurus plates, which is one of the most important active tectonic areas in the country. The reservoir was modelled by 3D numerical simulation-based analysis. Although this study is a case study, the most important original aspect of this study is the modelling of the cumulative effects of impulse waves triggered by two concurrent landslides in a dam reservoir, unlike other studies. The model includes a landslide on the left shore and another landslide on the right shore that are 800 m and 4900 m away from the dam body, respectively. The results obtained were evaluated and compared.

To accurately simulate the landslide deformation, a non-Newtonian fluid model was applied using the VOF technique with CFD code in the numerical model due to the complex rheology of landslide materials. In the first stage of the study, the occurrence of a subaerial landslide 800 m away from the dam body was simulated. The landslide material reached the reservoir 7 s after the slide formed a 15-m wave in the impact area. As the wave was moving towards the dam body, it was damped by colliding with a ridge extending towards the reservoir just west of the impact zone and reached the dam body with a wave height of 4 m at 34 s after the start of the slide.

In the second stage of the study, the occurrence of a partially submerged landslide 4900 m away from the dam body was simulated. The toe was submerged in the reservoir. The landslide completely slid into the reservoir after 12 s, and a 30-m wave was formed in the impact area. This wave reached the dam body after 205 s, and the wave height was 4.2 m. The main reasons for the decrease in the height of the wave after travelling for about 5 km in front of the dam body are the geometry of the reservoir, the angle between the sliding direction of the landslide and the travel direction of the resulting impulse wave in the reservoir, and especially the ridge extending into the reservoir just opposite the landslide mass.

In order to evaluate the holistic effect of the concurrent landslides, the simultaneous activation of both landslides was simulated. Impulse waves propagated towards each other and interfered with each other at 97 s after the beginning of the movements. It was expected that the impulse waves would dampen each other due to the turbulence and that the height of the wave that reached the dam body would decrease. At the end of 220 s, when the wave reached the dam body, its height reached 5.6 m. Table 2 shows the wave height and free water elevation values determined by the numerical analysis.

The general evaluations based on the results of this case study are summarized as follows. Impulse waves travelling along the reservoir lose energy depending on the reservoir topography, and their height and celerity naturally decrease with increasing travel distance. In front of the dam body, the impulse wave triggered by the landslide located further away from the dam is higher than the wave originating from the landslide located near the dam. The higher impulse wave triggered by the landslide has a travel distance of 6 times higher and a volume of only 3 times higher, which indicates that the volume of the landslide material sliding into the reservoir and wave propagation direction related to landslide location are more important than the travel distance regarding the impulse wave's height.

Wave interference occurred when two waves that were travelling in opposite directions meet. As the impulse waves

passed through each other, the crests combined and produced a wave with greater amplitude, and higher free-surface elevation was recorded. After the interference, the celerity of the impulse wave that continued to propagate towards the dam decreased, but its height increased by 1.4 m and reached 5.6 m. The impulse waves and the resultant reflected waves induced by the first (near) landslide constructively interfere with the impulse waves induced by the second (far) landslide, thus forming waves with higher amplitudes/heights.

When two water waves arrive at the same point, superposition occurs, resulting in merging of the waves. This event results in constructive or destructive interference because the waves consist of crests and troughs. Constructive interference occurs when the crests or troughs of two waves superimpose, and the resulting wave has a higher amplitude than the previous ones. Destructive interference occurs when the trough of a wave superimposes with the crest of another wave, and the waves cancel each other out, leading to lower amplitude. Although this is also true for impulse waves, the fact that a trough does not form in front of an impulse wave (Fig. 1) means that crests of the convergent waves interfere with each other. In this case, when two opposite impulse waves meet at the same point, constructive interference occurs, resulting in increased wave height. In this study, this result was seen very clearly.

The obtained results show that evaluating the effects of landslides in dam reservoir areas separately is not sufficient for dam safety. It is possible that concurrent landslides may occur at the same time, especially in reservoirs near tectonically active areas, as in this study. For this reason, effects of all landslides in the reservoir should be investigated, and numerical simulations should be performed, especially for the concurrent landslides considering different variations. Furthermore, changes in wave height and celerity should be determined, and the holistic effects of landslides should be evaluated.

Declarations

Conflict of interest The authors declare no competing interests.

References

- Abdollahi A, Mason HB (2019) Tsunami-induced pore water pressure response of unsaturated soil beds: numerical formulation and experiments. *Comput Geotech* 110:19–27. <https://doi.org/10.1016/j.compgeo.2019.02.012>
- Açıkbaş D, Akgül A, Erdoğan LT (1981) Güneydoğu Anadolu'nun hidrokarbon olanakları ve Baykan-Şirvan-Pervari yöresinin jeolojisi. TPAO Report, Ankara (in Turkish)
- Bazykina AY, Mikhailichenko SY, Fomin VV (2018) Numerical simulation of tsunami in the Black Sea caused by the earthquake on September 12, 1927. *Phys Oceanogr* 25:295–304. <https://doi.org/10.22449/1573-160x-2018-4-295-304>
- Bonaccorso A, Calvari S, Garfi G et al (2003) Dynamics of the December 2002 flank failure and tsunami at Stromboli volcano inferred by volcanological and geophysical observations. *Geophys Res Lett* 30:1–4. <https://doi.org/10.1029/2003GL017702>
- Bregoli F, Bateman A, Medina V (2017) Tsunamis generated by fast granular landslides: 3D experiments and empirical predictors. *J Hydraul Res* 55:743–758. <https://doi.org/10.1080/00221686.2017.1289259>
- Brethour JM, Hirt CW (2009) Drift model for two-component flows. *Flow Sci Inc* 1–7
- Choudhury D (1973) Introduction to the renormalization group method and turbulence modeling. Fluent Incorporated
- Day S, Llanes P, Silver E et al (2015) Submarine landslide deposits of the historical lateral collapse of Ritter Island, Papua New Guinea. *Mar Pet Geol* 67:419–438. <https://doi.org/10.1016/j.marpetgeo.2015.05.017>
- De-Girolamo P, Cecioni C, Montagna F et al (2009) Numerical modelling of landslide generated tsunamis around a Conical Island. In: *Proceedings of the Coastal Engineering Conference*, pp 1287–1299
- Di Risio M, De Girolamo P, Bellotti G et al (2009) Landslide-generated tsunamis runup at the coast of a conical island: new physical model experiments. *J Geophys Res Ocean* 114:1–16. <https://doi.org/10.1029/2008JC004858>
- Ersoy H, Karahan M, Gelişli K et al (2019) Modelling of the landslide-induced impulse waves in the Artvin Dam reservoir by empirical approach and 3D numerical simulation. *Eng Geol* 249:112–128. <https://doi.org/10.1016/j.enggeo.2018.12.025>
- Ersoy H, Karahan M, Öztürk HH (2020) Baraj Rezervuarlarında Heyelanlardan Kaynaklanacak İtki Dalga Özelliklerinin Ampirik İlişkilerle Değerlendirilmesi: Borçka Barajı Örneği. *DOAD* 6:248–257. <https://doi.org/10.21324/dacd.621377> (in Turkish with English abstract)
- Evers FM, Hager WH (2015) Impulse wave generation: comparison of free granular with mesh-packed slides. *J Mar Sci Eng* 3:100–110. <https://doi.org/10.3390/jmse3010100>
- Franco A, Moernaut J, Schneider-Muntau B, Strasser M, Gems B (2021a) Triggers and consequences of landslide-induced impulse waves—3D dynamic reconstruction of the Taan Fiord 2015 tsunami event. *Eng Geol* 294:106384. <https://doi.org/10.1016/j.enggeo.2021.106384>
- Franco A, Schneider-Muntau B, Roberts NJ, Clague JJ, Gems B (2021b) Geometry-based preliminary quantification of landslide-induced impulse wave attenuation in mountain lakes. *Appl Sci* 11:11614. <https://doi.org/10.3390/app112411614>
- Fritz HM, Hager WH, Minor HE (2004) Near field characteristics of landslide generated impulse waves. *J. Waterw. Port. Coast Ocean Eng* 130:287–302
- Fritz HM, Mohammed F, Yoo J (2009) Lituya bay landslide impact generated mega-tsunami 50th anniversary. In: Cummins PR, Satake K, Kong LSL (eds) *Tsunami science four years after the 2004 Indian Ocean Tsunami*. Pageoph Topical Volumes. Birkhäuser, Basel. https://doi.org/10.1007/978-3-0346-0064-4_9
- Gabl R, Seibl J, Gems B, Aufleger M (2015) 3-D numerical approach to simulate the overtopping volume caused by an impulse wave comparable to avalanche impact in a reservoir. *Nat Hazards Earth Syst Sci* 15:2617–2630. <https://doi.org/10.5194/nhess-15-2617-2015>
- Grilli ST, Vogelmann S, Watts P (2002) Development of a 3D numerical wave tank for modeling tsunami generation by underwater landslides. *Eng Anal Bound Elem* 26:301–313. [https://doi.org/10.1016/S0955-7997\(01\)00113-8](https://doi.org/10.1016/S0955-7997(01)00113-8)
- Heller V (2007) Landslide generated impulse waves: prediction of near field characteristics. ETH Zurich, Zürich (Dissertation)
- Heller V, Bruggemann M, Spinneken J, Rogers BD (2016) Composite modelling of subaerial landslide-tsunamis in different water body geometries and novel insight into slide and wave kinematics.

- Coast Eng 109:20–41. <https://doi.org/10.1016/j.coastaleng.2015.12.004>
- Heller V, Hager WH (2010) Impulse product parameter in landslide generated impulse waves. *J Waterw Port, Coast Ocean Eng* 136:145–155. [https://doi.org/10.1061/\(ASCE\)WW.1943-5460.0000037](https://doi.org/10.1061/(ASCE)WW.1943-5460.0000037)
- Heller V, Hager WH, Minor HE (2009) Landslide generated impulse waves in reservoirs: Basics and computation. *Mitteilungen der Versuchsanstalt für Wasserbau, Hydrol und Glaziologie an der Eidgenössischen Technische Hochschule Zürich* 1–172
- Hendron AJ, Patton FD (1987) The vaiont slide - a geotechnical analysis based on new geologic observations of the failure surface. *Eng Geol* 24:475–491. <https://doi.org/10.1139/t87-023>
- Hibiki T, Ishii M (2003) One-dimensional drift-flux model for two-phase flow in a large diameter pipe. *Int J Heat Mass Transf* 46:1773–1790. [https://doi.org/10.1016/S0017-9310\(02\)00473-8](https://doi.org/10.1016/S0017-9310(02)00473-8)
- Huang BL, Wang SC (2017) Wave attenuation mechanism of cross-plates applied in landslide-induced tsunami in river course. *J Mt Sci* 14:649–661. <https://doi.org/10.1007/s11629-016-4218-6>
- Hughes SA (1993) Physical models and laboratory techniques in coastal engineering. World Scientific
- Kafle J, Tuladhar BM (2018) Landslide-water interaction for partially submerged landslide. *J Nepal Math Soc* 1:22–29
- Karahan M, Ersoy H, Akgun A (2020a) A 3D numerical simulation-based methodology for assessment of landslide-generated impulse waves: a case study of the Tersun Dam reservoir (NE Turkey). *Landslides* 17:2777–2794. <https://doi.org/10.1007/s10346-020-01440-4>
- Karahan M, Ersoy H, Anilan T (2020b) İtki dalgalarının oluşumunda ölçek etkisi, hareket süresi ve çarpma hızının model deneyler ve 3 boyutlu nümerik simülasyonlarla değerlendirilmesi (in Turkish with English abstract). *GUFEBED* 10:514–525
- Kesseler M, Heller V, Turnbull B (2018) A laboratory-numerical approach for modelling scale effects in dry granular slides. *Landslides* 15:2145–2159. <https://doi.org/10.1007/s10346-018-1023-z>
- Kim G-B (2012) Numerical simulation of three-dimensional tsunami generation by subaerial landslides. Texas A&M University (Dissertation)
- Kocaman S, Ozmen-Cagatay H (2015) Investigation of dam-break induced shock waves impact on a vertical wall. *J Hydrol* 525:1–12. <https://doi.org/10.1016/j.jhydrol.2015.03.040>
- Li G, Chen G, Li P, Jing H (2019) Efficient and accurate 3-D numerical modelling of landslide Tsunami. *Water (switzerland)* 11:1–17. <https://doi.org/10.3390/w11102033>
- Li DQ, Ding YN, Tang XS, Liu Y (2021a) Probabilistic risk assessment of landslide-induced surges considering the spatial variability of soils. *Eng Geol* 283:105976. <https://doi.org/10.1016/j.enggeo.2020.105976>
- Li Y, Pang R, Xu B, Wang X, Fan Q, Jiang F (2021b) GPDEM-based stochastic seismic response analysis of high concrete-faced rock-fill dam with spatial variability of rockfill properties based on plastic deformation. *Comput Geotech* 139:104416. <https://doi.org/10.1016/j.compgeo.2021.104416>
- Liu PLF, Wu TR, Raichlen F et al (2005) Runup and rundown generated by three-dimensional sliding masses. *J Fluid Mech* 536:107–144. <https://doi.org/10.1017/S0022112005004799>
- Montagna F, Bellotti G, Di Risio M (2011) 3D numerical modeling of landslide-generated tsunamis around a conical island. *Nat Hazards* 58:591–608. <https://doi.org/10.1007/s11069-010-9689-0>
- Pang R, Xu B, Kong X, Zhou Y, Zou D (2018) Seismic performance evaluation of high CFRD slopes subjected to near-fault ground motions based on generalized probability density evolution method. *Eng Geol* 246:391–401. <https://doi.org/10.1016/j.enggeo.2018.09.004>
- Pang R, Xu B, Zhou Y, Song L (2021) Seismic time-history response and system reliability analysis of slopes considering uncertainty of multi-parameters and earthquake excitations. *Comput Geotech* 136:104245. <https://doi.org/10.1016/j.compgeo.2021.104245>
- Perinçek D (1980) IX. Bölge Hakkâri-Yüksekovaçukurca-Beytüşşebap-Uludere-Pervari dolayının jeolojisi. TPAO Report, Ankara (in Turkish)
- Perinçek D (1990) Hakkari ili ve dolayının stratigrafisi, GDA Türkiye (in Turkish). *Bull Turk Assoc Pet Geol* 2:21–68
- Perinçek D (2016) Cetin Baraj Gövdesi ve Dolayının Jeolojisi ve Heyelan Araştırması. *Türkiye Jeol Bülteni* 59:167–210
- Perinçek D, Günay Y, Kozlu H (1987) New observation on strike-slip faults in east and southeast Anatolia. In: 7th Biannual Petroleum Congress of Turkey, Ankara
- Quecedo M, Pastor M, Herreros MI (2004) Numerical modelling of impulse wave generated by fast landslides. *Int J Numer Methods Eng* 59:1633–1656. <https://doi.org/10.1002/nme.934>
- Shen Y, Whittaker CN, Lane EM, Power W, Melville BW (2022) Interference effect on tsunami generation by segmented seafloor deformations. *Ocean Eng* 245:110244. <https://doi.org/10.1016/j.oceaneng.2021.110244>
- Shi C, An Y, Wu Q et al (2016) Numerical simulation of landslide-generated waves using a soil-water coupling smoothed particle hydrodynamics model. *Adv Water Resour* 92:130–141. <https://doi.org/10.1016/j.advwatres.2016.04.002>
- Smith RC, Hill J, Collins GS et al (2016) Comparing approaches for numerical modelling of tsunami generation by deformable submarine slides. *Ocean Model* 100:125–140. <https://doi.org/10.1016/j.ocemod.2016.02.007>
- Spesivtsev P, Sinkov K, Osiptsov A (2013) Comparison of drift-flux and multi-fluid approaches to modeling of multiphase flow in oil and gas wells. In: WIT Transactions on Engineering Sciences, pp 89–99
- Tolun N (1954) Güneydoğu Anadolu'nun stratigrafisi ve tektoniği. MTA Report, Ankara (in Turkish)
- Utmanoğulları M (2012) Geology, subsurface geology and hydrocarbon possibilities of around of Şirvan Özpınar (Siirt). Çanakkale Onsekiz Mart University (Dissertation)
- Vacondio R, Mignosa P, Pagani S (2013) 3D SPH numerical simulation of the wave generated by the vajont rockslide. *Adv Water Resour* 59:146–156. <https://doi.org/10.1016/j.advwatres.2013.06.009>
- Wang J, Ward SN, Xiao L (2019) Tsunami Squares modeling of landslide generated impulsive waves and its application to the 1792 Unzen-Mayuyama mega-slide in Japan. *Eng Geol* 256:121–137. <https://doi.org/10.1016/j.enggeo.2019.04.020>
- Wang D, Wang Z, Li Y et al (2020) Characteristics and dynamic process analysis of the 2018 Mabian consequent landslide in Sichuan Province, China. *Bull Eng Geol Environ* 79:3337–3359. <https://doi.org/10.1007/s10064-020-01784-0>
- Wang W, Chen G, Yin K et al (2015) Modeling of landslide generated waves in Three Gorges Reservoir, China using SPH method. In: 15th Asian Regional Conference on Soil Mechanics and Geotechnical Engineering, ARC 2015: New Innovations and Sustainability, pp 1183–1188
- Xu WJ, Yao ZG, Luo YT, Dong XY (2020) Study on landslide-induced wave disasters using a 3D coupled SPH-DEM method. *Bull Eng Geol Environ* 79:467–483. <https://doi.org/10.1007/s10064-019-01558-3>
- Xu WJ, Wang YJ, Dong XY (2021) Influence of reservoir water level variations on slope stability and evaluation of landslide tsunami. *Bull Eng Geol Environ* 80:4891–4907. <https://doi.org/10.1007/s10064-021-02218-1>
- Yavari-Ramshe S, Ataie-Ashtiani B (2016) Numerical modeling of sub-aerial and submarine landslide-generated tsunami waves—recent advances and future challenges. *Landslides* 13:1325–1368. <https://doi.org/10.1007/s10346-016-0734-2>
- Yin YP, Huang B, Chen X et al (2015) Numerical analysis on wave generated by the Qianjiangping landslide in Three Gorges

- Reservoir, China. *Landslides* 12:355–364. <https://doi.org/10.1007/s10346-015-0564-7>
- Yılmaz Y, Yiğitbaş E (1990) GD Anadolu'nun farklı ofiyolitik-metamorfik birlikleri ve bunların jeolojik evrimdeki rolü (in Turkish). *Türkiye* 8:128–140
- Zhang T, Yan E, Cheng J, Zheng Y (2010) Mechanism of reservoir water in the deformation of Hefeng landslide. *J Earth Sci* 21:870–875. <https://doi.org/10.1007/s12583-010-0139-4>
- Zhang Y, Li D, Chen L et al (2020) Numerical analysis of landslide-generated impulse waves affected by the reservoir geometry. *Eng Geol* 266:1–15. <https://doi.org/10.1016/j.enggeo.2019.105390>
- Zhao T, Uti S, Crosta GB (2016) Rockslide and impulse wave modelling in the Vajont Reservoir by DEM-CFD analyses. *Rock Mech Rock Eng* 49:2437–2456. <https://doi.org/10.1007/s00603-015-0731-0>